Acoustic Performance Assessment of Sustainable Acoustic Absorbers Made from Olive Tree Pruning and Pine Waste

DOI: 10.61782/fa.2023.1218

forum acusticum 2023

ACOUSTIC PERFORMANCE ASSESSMENT OF SUSTAINABLE ACOUSTIC ABSORBERS MADE FROM OLIVE TREE PRUNING AND PINE WASTE

Rossella Cottone[*1,2,3] **Louena Shtrepi**[3] **Valentina Serra**[3]
Simonetta Lucia Pagliolico[4] **Alessandro Schiavi**[5]
[1] Department of Materials Engineering and Physics, Faculty of Civil Engineering, Slovak University of Technology, Bratislava, Slovakia
[2] Department of Architecture, Campus Brussels and Ghent, KU Leuven, Belgium
[3] Department of Energy, Politecnico di Torino, Italy
[4] Department of Applied Science and Technology, Politecnico di Torino, Italy
[5] INRiM - National Institute of Metrological Research, Applied Metrology and Engineering Division, Torino, Italy

ABSTRACT

This work aims to elaborate and characterize new ecological composite materials from olive trees pruning waste for the manufacture of acoustic absorbers. For this purpose, two samples' typologies of loose olive tree chips have been considered after applying different degrees of chipping and blending to olive pruning waste. The samples have been compared to a third sample based on pine shavings waste. Firstly, the morphological analysis of the different samples was carried out by micro computed tomography (Micro-CT) scanning. Secondly, the acoustic properties were measured experimentally using impedance tube method, and assessed from air flow resistivity and permeability; the mass transport properties are exploited for the characterization of microstructural parameter, such as tortuosity, effective porosity and pore structure morphology by applying analytical models for fibrous and granular materials. The experimental results demonstrated that the samples, for the given thickness, have single third-octave band sound absorption values that can reach higher values than 0.50 above 1000 Hz. A good match between experimental and analytical models could be found.

[*] ***Corresponding author***: rossella.cottone@stuba.sk

Keywords: *olive tree pruning chips, pine shavings, loose materials, sound absorption coefficient, microstructural properties.*

1. INTRODUCTION

Several studies have shown the advantage of the use of inorganic materials to achieve indoor acoustic comfort. However, the use of natural materials is advantageous for the reduction of the embodied energy of the building sector and achievement of a sustainable development for both economic and environmental perspectives. In addition, materials from renewable or naturally occurring resources have come close in performance to conventional sound-absorbing surface treatments made from synthetic fibers, but with a considerable reduced production costs, lighter weight, and higher degree of biodegradation [1]. Despite considerable investigations and interest on natural materials, there is little research on the reuse of agricultural waste, specifically, olive tree by-product, which can be used as acoustically absorbent materials.

The purpose of this work is two folded. First of all, it aims to put attention on the use of agricultural by-products as sound-absorbing materials to promote a circular economy and clean production [2], and secondly, to address an environmentally critical situation, namely the burning of olive tree prunings in agricultural fields. Indeed, all areas of the Mediterranean have significant cultivation of olive groves, which during the pruning phase of production

generates a large amount of waste that, in most cases, is burned in the fields, worsening the current climatic conditions.

The main goal of this research is to give to loose material based on olive tree branches and leaves waste a second life by recycling and converting them into a high-value resource, i.e., a by-product to be used for the production of sound-absorbing panels. The loose material has been analyzed in a few studies in which only olive leaves or differentiated wood have been examined, considering traditional measurements based on the impedance tube method [3, 4]. Furthermore, loose waste derived from olive tree pruning wood has never been tested in the totality of its properties, apart from two research studies in which parameters, such as air flow resistivity (σ) and porosity (ε), were measured for olive leaves bonded with chitosan glue [4]. In addition, the acoustic behavior of the olive tree pruning waste was for the first time characterized, taking into consideration its aesthetic design value, in a previous research by the authors [5].

The aim of this research is to process and characterize loose wood chips derived from olive tree pruning providing the sound absorption values through the impedance tube method [6], and the intrinsic microstructural and mass transport properties such as tortuosity, porosity, airflow resistivity, and permeability, by micro computed tomography (Micro-CT) scanning [7] and by experimental pressure wave drop assessment [8]. Moreover, the authors have added for comparisons a further typology of loose material with comparable maximum particle size but different density than olive wood chips, that is the pine shavings waste obtained in carpentry workshops, in order to assess the influence of chipping in microstructural and absorption parameters of two wood species.

2. MATERIAL AND METHODS

2.1 By-products of olive tree pruning wood chips and pine shavings

Two different materials, olive pruning wood chips and pine shavings, were analyzed. In particular, three samples, CC, CF and P, were characterized. The first one (CC) was obtained from the manual pruning of the cultivar Cerasuola, one of the oldest in western Sicily. The pruned branches and leaves were processed indistinctly, using a professional model chipper, into the by-product consisting of wood chips, which was then sieved to remove the coarser fraction and obtain a maximum wood chip size (d) between 4 mm and 10 mm (Figure 1a). The prunings were then dried in a ventilated oven at 103°C to obtain a normal moisture content to prevent the material from being attacked by mold or insects. After the drying phase, the bulk density was calculated as given in Sec. 2.1. of [5], observing a density of about 280±12 kg/m^3. Next, the same type of by-product was blended to obtain the sample CF with a particle size smaller than the CC sample, i.e., $1 < d < 6.5$ mm, and a density of 350±10 kg/m^3 (Figure 1b).

The carpentry workshop by-product, namely pine shavings (Figure 1c) have a maximum particle size (d) between 3 mm and 8 mm with a density of about 55±11 kg/m^3, measured by the same methodology as olive wood chips expressed in the Sec. 2.1. of [5], and a moisture content of 7%. Table 1 summarizes the characteristics of the different by-products.

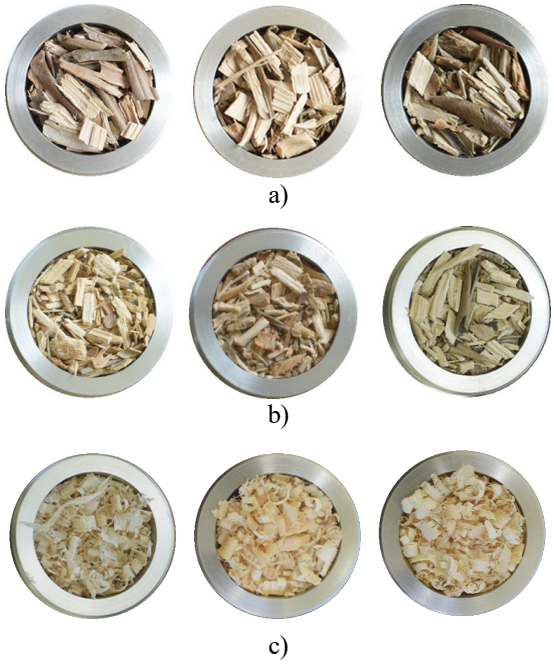

Figure 1. Samples of loose materials placed into the impedance tube. a) olive tree wood chips (CC); b) blended olive tree wood chips (CF); pine shavings (P).

Table 1. Characteristics of the by-products.

By-product	***Sample***	***Maximum particles size* [mm]**	***Density of loose material* [kg/m^3]**	***Moisture content* [%]**
Olive tree pruning chips	**CC**	$4 < d < 10$	280±12	~10
Blended olive tree pruning chips	**CF**	$1 < d < 6.5$	350±10	~10
Pine shavings	**P**	$3 < d < 8$	55±11	~7

2.2 Microstructural and transport properties characterization

2.2.1 μ-CT scanning

μ-CT scanning was performed in air on a Custom-built Computed Tomography (Fraunhofer IKTS, Dresden, Germany) at the research center for advanced joining technologies J-Tech@POLITO (Politecnico di Torino).
Projection images were collected using a source voltage of 100 kV and a source current of 140 μA, without X-ray filter. A 6-fold magnification was used providing a voxel size of 33.33 μm. The rotation step size was set with an angular increment of 0.225° and with an exposure time of 1s for each scan. Four images were integrated for each rotation step. Before reconstruction, a translational motion compensation was performed to avoid mismatching between the 0◦ and the 360◦ shadow images in case of a slight sample movement during the data collection. This compensation, the reconstruction of virtual volumes, and the structural features of the samples were performed in the software VGStudio Max 3.5 software (Volume Graphics, Heidelberg, Germany) based on the Cauchy-Crofton approach. Apart from the main software, the add-on modules Porosity/inclusion analysis and Foam/powder analysis were used. A virtual parallelepiped was used to extract an internal part of the reconstructed volume to avoid the effects of the irregular contours of the samples and establish a reference volume for the calculations. The parallelepiped was extracted as a separate reference virtual volume and an isovalue-based surface determination procedure was run. Porosity/inclusion analysis module was used to determine the void fraction ε of samples as the ratio of the void volume to the total volume. Foam/powder analysis module was used to extract sample structure data employing a merge threshold of 70% and a standard precision procedure. The module allows the segmentation of CT data into separate void cells which can be visualized and statistically analyzed. In the same way, the strut thickness between void cells can be quantified and analyzed.
To characterize the microstructure of the samples, the following parameters were examined:

- the equivalent void diameter D_{eq} - the diameter of a sphere that has the same volume as the single void cells;
- the strut thickness St - the diameter of the maximum sphere inscribed in the solid space;
- the void sphericity φ - the ratio between the surface of a sphere with the same volume as the void cell and the surface of the cell.

2.2.2 Air flow resistivity

The experimental technique to evaluate the airflow resistivity is based on the generation of an alternating air flow through the material, according to ISO Standard 9053-2:2020 [9] and literature [10, 11]; the occurring pressure wave drop is accurately measured using a low-frequency capacitive microphone (B&K, type 4193). The airflow resistivity is determined on the basis of the ratio between the RMS value of the pressure wave drop, and the RMS value of the volumetric airflow. Using the alternating flow method, the airflow resistivity is determined on the basis of the following relationship:

$$r = \frac{p_{RMS}}{q_{RMS}} \cdot \frac{A}{L} \quad [\text{Pa}\cdot\text{s}\cdot\text{m}^{-2}] \qquad (1)$$

Where p_{RMS} is the RMS value of the pressure wave drop /Pa, q_{RMS} is the RMS value of the alternating volumetric airflow /$\text{m}^3\cdot\text{s}^{-1}$, A is the surface area of the sample/m^2, and L is the thickness of the sample/m. In particular, p_{RMS} is the value of the sinusoidal pressure component, $p_{RMS}=\gamma p_0 \partial V (V_0\sqrt{2})^{-1}$, which depends on the atmospheric static pressure p_0 (with heat capacity ratio γ =1.4), and on the air volume variation ∂V, occurring in the volume of air V_0, due to the imposed alternating air flow. The amplitude of the sinusoidal pressure component is measured by a microphone, with known sensitivity in mV/Pa; the alternating volumetric air flow, $q_{v,RMS}=\omega \partial V (\sqrt{2})^{-1}$, depends on the angular frequency of oscillation ω, and the corresponding volume variation ∂V of the given air volume V_0. Therefore, by combining the quantities above described, the airflow resistivity r, is obtained from the following physical model:

$$r = \frac{\gamma p_0}{\omega V_0} \cdot \frac{A}{L} \cdot \zeta \quad [\text{Pa}\cdot\text{s}\cdot\text{m}^{-2}] \qquad (2)$$

where ζ is the experimental ratio between the indication of the microphone in mV/Pa, of the amplitude of the pressure wave drop, during compression and rarefaction ∂V of the air volume V_0 through the porous material, and the microphone sensitivity in mV/Pa. Figure 2 shows the principle of measurement.

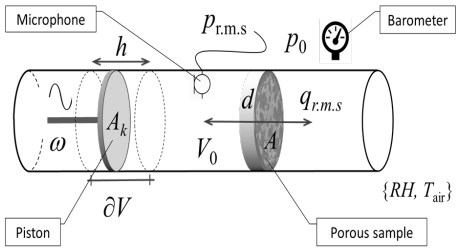

Figure 2. The physical principle of the alternating airflow measurement.

The value ∂V depends on the area A_k of the piston and its stroke h. For this measuring system A_k=1.9·10^{-3} m^2 and h=1.7·10^{-3} m, therefore ∂V = 3.23·10^{-6} m^3. Furthermore, depending on the type and geometry of the material examined, it is necessary to vary the speed of the flow, in order to maintain conditions of laminar flow. This can be done by acting on the length of the stroke h or by varying the angular frequency ω. In particular, with this apparatus it is possible to vary the angular velocity ω between 0.63 rad/s and 12.6 rad/s (that is, between 0.1 Hz and 2 Hz).

2.3 Impedance tube method

The measurements of the sound absorption coefficient in normal incidence (α_N) are carried out using the impedance tube in accordance with ISO 10534-2:2001 [6]. Figure 3 shows the diagram operation of the tube used, which consists of a loudspeaker tied to the impedance tube, three microphones placed at two different distances, as well as 65 mm and 29 mm, a rigid termination within which the test specimen is placed, and a movable plunger to push the specimen flush between the rigid termination and the impedance tube.

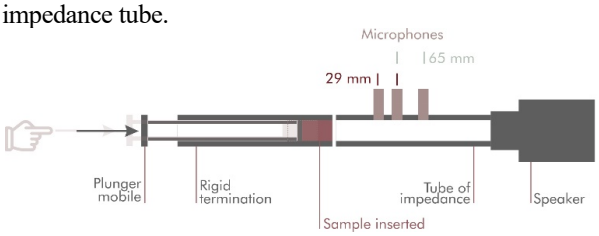

Figure 3. Diagram of the impedance tube used for the measurements.

This method is based on the calculation of the transfer function between the signal that is detected by the two microphones used when the impedance tube is stressed by the loudspeaker placed at the end. According to the standard, the loudspeaker generates white noise and produces plane waves, and by measuring the sound pressure at the points where microphones are placed, absorption coefficient in normal incidence is calculated.
The distance between the two microphones in the measurements setup was 29 mm. This distance sets the lower limit frequency according to the ISO standard [6]. Considering the inner diameter of the tube and the distance between the two microphones, the frequency range in which the measurement of the absorption coefficient at normal incidence is valid is 119 Hz < f < 5700 Hz.

The materials investigated are loose, so in order to measure the coefficient at normal incidence, it was necessary to place the experimental device vertically, which was then filled with the loose material with a thickness of 40 mm.

3. RESULTS AND DISCUSSION

3.1 Microstructural properties

Figure 4a) is an example of µ-CT image that shows the reference volume of sample CC (Table 2). This portion of volume was considered for microstructural analysis, being representative of the reconstructed volume of the sample and free of any effect due to the chips orientation close to the walls of the sample holder. The presence of voids was evaluated in 2D sections using the Porosity/Inclusion module. Figure 4b) shows the image of a section perpendicular to the y-axis (green colored section of the reference volume visible in the upper left panel). Table 2 shows the numerical values of the reference volumes for each sample, the volume of solid and void, evaluated excluding the micropores within the wooden chips, and the void fraction. Table 3 shows the microstructural parameters evaluated with the Foam/Powder module: the expected values (E) of the equivalent diameter of the voids (D_{eq}), considered as virtual closed cells, the thickness of the solid struts (St), the sphericity of the voids (φ), and their respective minimum (m) and maximum (M) values and standard deviations (σ).
Figure 5a) shows the enlarged µ-CT section of an olive wood chip. The micropores (dark dots), ranging in size from 1 µm to 100 µm, correspond to the vessels of deciduous wood [12, 13]. Figure 5b) is a courtesy image of the CNR-IBE Archive [14] showing the cross section (TS) of the wood of Olea Europea L. and the morphology of the vessels.

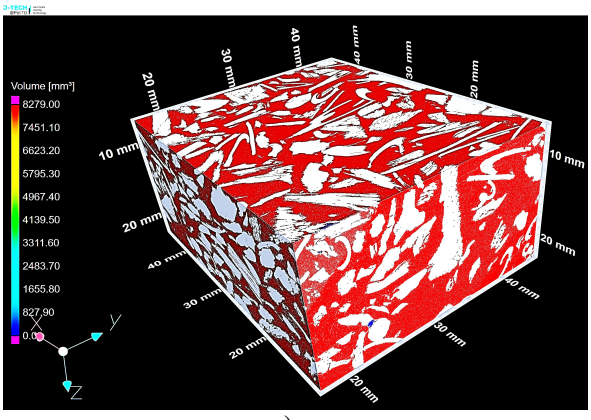

a)

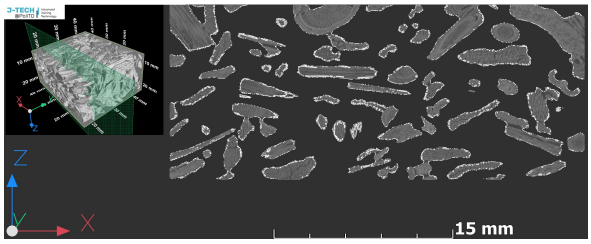

b)

Figure 4. µ-TC images of sample CC: a) the reference volume; b) a section of the reference volume (top left box).

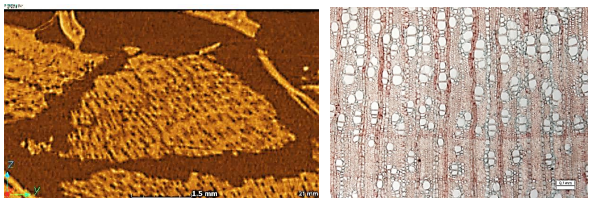

a) b)

Figure 5. a) µ-CT magnification of an olive wood chip (non-TS); b) TS of Olea europea L. wood in transmitted light microscopy. In evidence the vessels (image courtesy of the Archivio CNR-IBE [14]).

Settling of loose wood chips inside the holder creates a single structure made up of disjointed lumps, having an open pore morphology and a broad distribution of both the dimensions of voids and their sphericities. Figures 6 and 7 respectively show the distribution of the equivalent diameter of voids and the graph of sphericity versus the equivalent diameter of voids for sample CC. The $\varphi_{E(Deq)}$ in Table 3 is the value of the polynomial trendline shown in Figure 7 for $D_{eq} = E(D_{eq})$, and (min; max) are the minimum and maximum fluctuations of φ at $D_{eq} = E(D_{eq})$. Majority of voids of CC sample shows low sphericity (φ = 0.23-0.33) and most of the larger voids exhibit the lowest sphericity. Samples CF and P also show low sphericities, 0.25 and 0.36 respectively, and slightly wider distributions around the mean value than CC. As with sample CC, the largest voids of samples CF and P show the lowest sphericity.

Table 2. µ-CT void fraction data by the Porosity/inclusion analysis on the reference volumes.

Sample	*Ref. volume* [mm³]	*Solid volume* [mm³]	*Void volume* [mm³]	*ε* [%]
CC	10197	5213	4983	48.87
CF	3504	1875	1628	46.47
P	20883	1815	19068	91.31

Table 3. µ-CT microstructural data by the Foam/powder analysis on the reference volumes (see table 2).

Sample	*D_{eq}*			*St*			*φ*
	$E(D_{eq})$ [µm]	*m; M* [µm]	*σ* [µm]	*E(St)* [µm]	*m, M*	*σ* [µm]	*$\varphi_{E(Deq)}$* (min; max)
CC	2381	41; 5334	829	956	0; 3379	610	0.27 (0.23÷0.33)
CF	859	41; 2457	321	258	0;1231	197	0.25 (0.16÷0.36)
P	1642	280; 5229	664	118	0; 514	71	0.36 (0.25÷0.49)

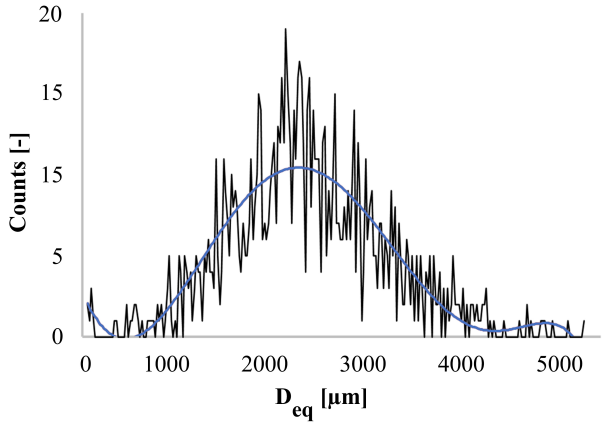

Figure 6. CC void equivalent diameter distribution and polynomial trendline (n=6; R^2=0.74).

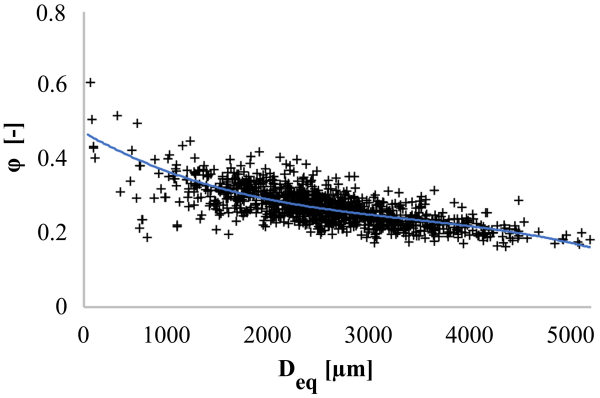

Figure 7. Sphericity vs. void equivalent diameter and polynomial trendline (n=3; R^2 = 0.51).

3.2 Mass transport properties

3.2.1 Air flow resistivity, porosity and tortuosity

Airflow resistivity is an intrinsic material property, independent of the physical properties of the flow fluid used, such as dynamic viscosity μ, density ρ, and also independent of gravitational field g. Indeed, once the airflow resistivity r of a given material is known, it is possible to derive other quantities relating to the mass transport properties, such as the intrinsic permeability k and the hydraulic conductivity K_g for different types of fluid, by means of simple calculations, e.g., $k=\mu/r$ e $K_g=\rho g/r$.
These parameters can be exploited to evaluate several physical and mechanical features of the investigated materials (here not discussed), such as moisture diffusivity, moisture vapor transfer, breathability, infiltration rate, and other parameters of interest in building physics applications. Measurements of airflow resistivity, performed according the procedure described in Sec. 2.3.2, are carried out by filling specific holders by the loose wood chips of investigated materials. As a first step, the airflow resistivity of the empty holder (since it is closed upward and downward by two grids), is measured, in order to assess the threshold baseline (namely, 0.16 kPas/m^2). Then, the airflow resistivity of the loose wood chips is quantified, as a function of apparent density of the sample under investigation. In the Table 4, the experimental results are summarized.

Table 4. Mass transport properties of the investigated materials. Airflow resistivity r, permeability k, hydraulic conductivity K_g, and related standard deviations σ.

Sample	r [kPas/m^2]	$\sigma(r)$	k [m^2]	$\sigma(k)$	K_g [m/s]	$\sigma(K_g)$
CC	1.8	0.1	$1.0\cdot10^{-8}$	$3.4\cdot10^{-10}$	5.6	0.2
CF	6.5	0.3	$2.8\cdot10^{-9}$	$1.2\cdot10^{-10}$	1.5	0.1
P	1.5	0.1	$1.2\cdot10^{-8}$	$1.8\cdot10^{-10}$	6.5	0.1

In order to assess the pore interconnectivity and the open pore morphology, the porosity and the tortuosity of the loose wood chips samples, are determined. In particular, the pore tortuosity τ_p is calculated on the basis of a semi-empirical model proper for wood chips [15]. The model, based on a logarithmic function of porosity ε_0, is widely adopted and consistent with other studies [16, 17], returning the value of pore tortuosity as $\tau_p=1-1.6\cdot\ln(\varepsilon_0)$. In this case, the values of total porosity are determined from materials density ρ_{mat}, and actual bulk density ρ_{bulk}, since the porosity calculated by µ–CT does not account for the micropores (vessels) within the wood chips (1 -100 µm) and of the volume of the peripheral portion of the sample, as specified in Section 3.2. In this portion the porosity could be greater due to the uneven settling of the chips near the walls of the holder. Hence the total porosity is calculated as $\varepsilon_0=1-(\rho_{bulk}/\rho_{mat})$. The values of the solid phase material density are available in literature, in terms of 880 kg/m^3 for olive wood [12], and 430 kg/m^3 for pine wood [18]. Since the uncertainties of these values are unknown, a precautionary range of 20% is considered in calculation. In Table 5 the values of investigated samples bulk density, total porosity and tortuosity, are shown.

Table 5. Pore morphological features, in terms of total porosity ε_0, (calculated from densities ratio), and pore tortuosity τ_p, with related standard deviations σ.

Sample	ρ_{bulk} [kg/m^3]	$\sigma(\rho)$ [kg/m^3]	ε_0 [%]	$\sigma(\varepsilon_0)$ [%]	τ_p [-]	$\sigma(\tau_p)$ [-]
CC	250.6	0.5	73.7	7.2	1.490	0.155
CF	309.7	0.3	67.4	9.7	1.631	0.156
P	52.7	0.3	87.8	2.8	1.209	0.045

The accurate determination of these non-acoustical parameters allows the implementation of suitable semi-empirical models [19,20] to calculate the sound absorption in granular disperse materials, such as loose wood chips, and to improve their performance, by engineering the shape, the arrangement, and the distribution. The Miki model [20] has been used in this work and compared to experimental data of sound absorption coefficients as measured in the following section.

3.3 Sound absorption coefficient

For the calculation of third-octave bands sound absorption values using the impedance tube (α_N), three samples were made from the same by-product, using the same amount of loose material, the same thickness, and the same operator for realization, in order to assess the contribution to uncertainty due to reproducibility. In addition, three measurement repetitions were carried out for each sample in order to assess the repeatability of the data [21, 22], for a total of 9 measurements finding compatibility between measurements on the different samples. Figure 8 shows the frequency sound absorption curves of the three samples CC, CF and P (see Figure 1 a, b, c, respectively) as the averages of the 9 measurements with the evaluation of the uncertainty expressed by the error bar.
Sample CC recorded negligible sound absorption values at mid to low frequencies in the range 100 - 1000 Hz, but recorded an initial peak maximum at 1600 Hz with a value

almost equal to 0.70 and then decreasing linearly reaching a minimum peak between 2500 - 3150 Hz with a value of about 0.40. The curve then rises linearly until 5000 Hz reaching a second peak with an absorption value of 0.85. The blended sample CF also obtained negligible sound absorption values at the mid to low frequencies in the range 100 - 800 Hz, but recorded a first peak maximum between 1250 - 1600 Hz with a value almost equal to 1 and then fell linearly reaching a peak minimum between 2500 - 3150 Hz with a value of about 0.50. The curve then increases linearly until 5000 Hz reaching a second peak with an absorption value of 0.90. Finally, even in the case of the pine sample (P), sound absorption values were recorded to be negligible at the mid to low frequencies in the range 100 to 1000 Hz, but recorded a first peak maximum at 2000 Hz with a value of 0.70 and then decreasing linearly reaching a peak minimum at 3150 Hz with a value of about 0.50. The curve then increases linearly until 5000 Hz reaching a second peak with an absorption value of 0.80. The results discussed here demonstrated the compatibility of the data with the Miki analytical model [20].

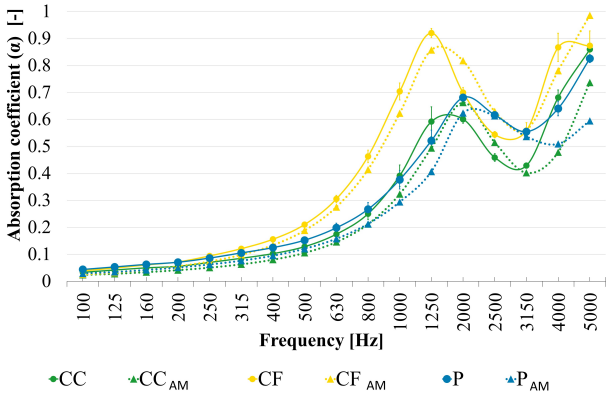

Figure 8. The sound absorption coefficients at normal incidence obtained from the measurement in the impedance tube CC, CF and P, and from the analytical model CC $_{AM}$, CF $_{AM}$, P $_{AM}$ [20].

4. CONCLUSIONS

Olive tree pruning chips and pine wood shavings were used in this work as a renewable resource to produce an environmental friendly sound-absorbing material and to promote the reuse of agricultural pruning and carpentry waste. The samples consist of loose wood chips with an open-pore structure and a broad distribution of both void size and morphology. As expected, most of the larger voids exhibit the lowest sphericity.

From the instrumental analysis, the single third-octave band sound absorption values of the three samples analyzed were obtained, showing that considering a thickness of 40 mm for all three cases negligible absorption was recorded at low frequencies. On the other hand, the samples can reach values above 0.50 from 1000 Hz onward with a maxima at frequencies range 1250-2000 Hz, and the minimum at 3150 Hz. These results demonstrate the possibility of reusing the two types of waste analyzed to produce innovative and sustainable sound-absorbing materials. In addition, the samples obtained have a wide range of uses. Different samples bound with natural glue will be realized and further evaluated, to define the effect of the binder on the loose materials and for a wall or ceiling application of solid panels in shape. Furthermore, more accurate models could be compared with the measured data in order to define the most appropriate one for the specific loose material.

5. ACKNOWLEDGMENTS

The authors would like to thank DONNAFUGATA S.r.l. Agricultural Society for the olive tree pruning chippings, Falegnameria Cucchiara for pine shavings waste, and the research center for advanced joining technologies J-Tech@POLITO (Politecnico di Torino) for µ–CT analyses.

6. REFERENCES

[1] Arenas, J. P., & Sakagami, K. (2020). Sustainable Acoustic Materials. Sustainability, 12(16), 6540. https://doi.org/10.3390/su12166540

[2] Fico, D., Rizzo, D., De Carolis, V., Montagna, F., Palumbo, E., & Corcione, C. E. (2022). Development and characterization of sustainable PLA/Olive wood waste composites for rehabilitation applications using Fused Filament Fabrication (FFF). Journal of Building Engineering, 56, 104673. https://doi.org/10.1016/j.jobe.2022.104673

[3] Bousshine, S., Ouakarrouch, M., Bybi, A., Laaroussi, N., Garoum, M., & Tilioua, A. (2022). Acoustical and thermal characterization of sustainable materials derived from vegetable, agricultural, and animal fibers. Applied Acoustics, 187, 108520. https://doi.org/10.1016/j.apacoust.2021.108520

[4] Martellotta, F., Cannavale, A., De Matteis, V., & Ayr, U. (2018). Sustainable sound absorbers obtained from olive pruning wastes and chitosan binder. Applied

Acoustics, 141, 71–78. https://doi.org/10.1016/j.apacoust.2018.06.022.

[5] Cottone, R., Shtrepi, L., Serra, V., & Pagliolico, S. L. (2023). The Recycling and Reuse of Natural Materials: Sound Absorbing Box Patterns That Use Waste from Olive Tree Pruning. Acoustics, 5(1), 177–192. https://doi.org/10.3390/acoustics5010011C

[6] ISO 10534-2:1998, Acoustics - Determination of sound absorption coefficient and impedance in impedance tubes - Part 2: Transfer-function method. International Organization for Standardization, Geneva, Switzerland.

[7] du Plessis, A., Broeckhoven, C., Guelpa, A., & le Roux, S. G. (2017). Laboratory x-ray micro-computed tomography: a user guideline for biological samples. GigaScience, 6(6), 1–11. https://doi.org/10.1093/gigascience/gix027

[8] Fiume, E., Schiavi, A., Orlygsson, G., Bignardi, C., Verné, E., & Baino, F. (2021). Comprehensive assessment of bioactive glass and glass-ceramic scaffold permeability: experimental measurements by pressure wave drop, modelling and computed tomography-based analysis. *Acta biomaterialia*, *119*, 405–418. https://doi.org/10.1016/j.actbio.2020.10.027

[9] ISO 9053-2:2020. Acoustics — Determination of airflow resistance — Part 2: Alternating airflow method

[10] Schiavi, A., Guglielmone, C., Pennella, F., & Morbiducci, U. (2012). Acoustic method for permeability measurement of tissue-engineering scaffold. Measurement Science and Technology, 23(10), 105702. https://doi.org/10.1088/0957-0233/23/10/105702

[11] Schiavi, A., Fiume, E., Orlygsson, G., Schwentenwein, M., Verné, E., & Baino, F. (2022). High-reliability data processing and calculation of microstructural parameters in hydroxyapatite scaffolds produced by vat photopolymerization. Journal of the European Ceramic Society, 42(13), 6206–6212. https://doi.org/10.1016/j.jeurceramsoc.2022.06.022

[12] Grioui, N., Halouani, K., Zoulalian, A., & Halouani, F. (2007). EXPERIMENTAL STUDY OF THERMAL EFFECT ON OLIVE WOOD POROUS STRUCTURE DURING CARBONIZATION. Maderas. Ciencia y Tecnología, 9(1). https://doi.org/10.4067/S0718-221X2007000100002

[13] Ehrlich Y, Regev L, Boaretto E. Discovery of annual growth in a modern olive branch based on carbonisotopes and implications for the Bronze Age volcanic eruption of Santorini. Scientific Reports 2021;11:704. https://doi.org/10.1038/s41598-020-79024-4 PMID: 33436660148.

[14] Archivio CNR-IBE, Sesto Fiorentino (FI), Italy.

[15] Comiti, J., & Renaud, M. (1989). A new model for determining mean structure parameters of fixed beds from pressure drop measurements: application to beds packed with parallelepipedal particles. *Chemical Engineering Science*, *44*(7), 1539-1545. https://doi.org/10.1016/0009-2509(89)80031-4

[16] Bo-Ming, Y., & Jian-Hua, L. (2004). A geometry model for tortuosity of flow path in porous media. *Chinese Physics Letters*, *21*(8), 1569.

[17] Ghanbarian, B., Hunt, A. G., Ewing, R. P., & Sahimi, M. (2013). Tortuosity in porous media: a critical review. *Soil science society of America journal*, *77*(5), 1461-1477. https://doi.org/10.2136/sssaj2012.0435

[18] Kantieva, E., Snegireva, S., & Platonov, A. (2021). Formation of density and porosity of pine wood in a tree trunk. IOP Conference Series: Earth and Environmental Science, 875(1), 012016. https://doi.org/10.1088/1755-1315/875/1/012016

[19] Cobo, P., & Simón, F. (2016). A comparison of impedance models for the inverse estimation of the non-acoustical parameters of granular absorbers. *Applied Acoustics*, *104*, 119-126. https://doi.org/10.1016/j.apacoust.2015.11.006

[20] Miki, Y. (1990). Acoustical properties of porous materials-Modifications of Delany-Bazley models. *Journal of the Acoustical Society of Japan (E)*, *11*(1), 19-24. https://doi.org/10.1250/ast.11.19

[21] ISO 12999-2:2014, "Acoustics - Determination and application of measurement uncertainties in building acoustics - Part 2: Sound absorption coefficients", 2014.

[22] JCGM 100, "Evaluation of measurement data — Guide to the expression of uncertainty in measurement", 2008.